ADVANCES IN ATMOSPHERIC SCIENCES, VOL. 38, JULY 2021, 1197–1208

• **Original Paper** •

# Three-Year Observations of Ozone Columns over Polar Vortex Edge Area above West Antarctica

Yuanyuan QIAN[1,2], Yuhan LUO[*1], Fuqi SI[1], Taiping YANG[1], and Dongshang YANG[1]

[1]*Key Laboratory of Environmental Optical and Technology*, *Anhui Institute of Optics and Fine Mechanics*, *Hefei Institutes of Physical Science*, *Chinese Academy of Sciences*, *Hefei* 230031, *China*

[2]*University of Science and Technology of China*, *Hefei* 230026, *China*

(Received 21 July 2020; revised 29 December 2020; accepted 11 February 2021)

ABSTRACT

Ozone vertical column densities (VCDs) were retrieved by Zenith Scattered Light-Differential Optical Absorption Spectroscopy (ZSL-DOAS) from January 2017 to February 2020 over Fildes Peninsula, West Antarctica (62.22°S, 58.96°W). Each year, ozone VCDs started to decline around July with a comparable gradient around 1.4 Dobson Units (DU) per day, then dropped to their lowest levels in September and October, when ozone holes appeared (less than 220 DU). Daily mean values of retrieved ozone VCDs were compared with Ozone Monitoring Instrument (OMI) and Global Ozone Monitoring Experiment 2 (GOME-2) satellite observations and the Modern-Era Retrospective analysis for Research and Applications Version 2 (MERRA-2) reanalysis dataset, with correlation coefficients ($R^2$) of 0.86, 0.94, and 0.90, respectively. To better understand the causes of ozone depletion, the retrieved ozone VCDs, temperature, and potential vorticity (PV) at certain altitudes were analyzed. The profiles of ozone and PV were positively correlated during their fluctuations, which indicates that the polar vortex has a strong influence on stratospheric ozone depletion during Antarctic spring. Located at the edge of polar vortex, the observed data will provide a basis for further analysis and prediction of the inter-annual variations of stratospheric ozone in the future.

**Key words:** ozone VCDs, ZSL-DOAS, Antarctic ozone depletion, polar vortex

**Citation:** Qian, Y. Y., Y. H. Luo, F. Q. Si, T. P. Yang, and D. S. Yang, 2021: Three-year observations of ozone columns over polar vortex edge area above West Antarctica. *Adv. Atmos. Sci.*, **38**(7), 1197−1208, https://doi.org/10.1007/s00376-021-0243-7.

**Article Highlights:**

- The ozone VCDs retrieved by ground-based ZSL-DOAS indicated that ozone holes appeared over the Fildes Peninsula, West Antarctica, with sharp fluctuations during the spring.
- The polar vortex has a strong influence on stratospheric ozone depletion during Antarctic spring.
- The ozone VCDs from ground-based observations validate satellite observations over the Fildes Peninsula.

## 1. Introduction

Ozone is an important trace gas in the Earth's atmosphere that impacts the environment, climate change, and human health (Li et al., 2015). It is most prevalent about 20−35 km above the surface of the Earth, where it can absorb UV radiation to protect life on Earth. The ozone hole was first discovered by Farman in Argentine Islands (65°S, 64°W) and Halley Bay (76°S, 27°W), Antarctica (Farman et al., 1985). Long-term trends in ozone column measurements, obtained from South Pole stations and Solar Backscatter Ultra Violet (SBUV) satellite observations, indicate that healing of Antarctic ozone holes is occurring based on control of Hydrochlorofluorocarbons emissions (Solomon et al., 2016).

Accurate retrieval of ozone columns, as well as comprehensive analysis of stratospheric chemistry, dynamics and temperature changes on ozone columns is necessary for the analysis of Antarctic ozone changes. Ozone columns over Antarctica are mainly obtained from satellite observations, ground-based DOAS observations, Brewer spectrophotometers, and Dobson spectrophotometers (Čížková et al., 2019; Kokhanovsky et al., 2020). Satellite observations and European Centre for Medium-Range Weather Forecasts (ECMWF) data were analyzed to study the influence of stratospheric halogen species (mainly Cl and Br) in the polar vortex, which may lead to ozone depletion over Antarctica (Mars-

* Corresponding author: Yuhan LUO
Email: yhluo@aiofm.ac.cn

ing et al., 2019; Nakajima et al., 2020). In addition, an atmospheric and chemical transport model is used for the analysis of long-term ozone trends and troposphere-stratosphere exchange in Antarctica (Hegglin and Shepherd, 2009; Lu et al., 2019).

The atmosphere over Antarctica is controlled by the strong polar vortex in winter, making it difficult to exchange with mid-latitude atmosphere. The extremely low air temperatures (< −78°C) inside the polar vortex, lead to the formation of polar stratospheric clouds (PSCs). PSCs, composed of nitrate trihydrate, water ice, etc., provide surfaces for heterogeneous reactions that convert halogen reservoirs to active halogens causing severe ozone depletion (Frieβ et al., 2005; Drdla and Müller, 2012; Marsing et al., 2019). There are three types of PSCs (decided by their state), including nitric acid trihydrate (NAT), supercooled ternary solution (STS), and ice PSCs, and their corresponding temperatures are $T_{nat}$ (−78°C), $T_{sts}$, and $T_{ice}$. The observation site is located at the edge of the polar vortex, which is different from other inland stations (high latitudes) where the ozone columns continued to be low in spring. The rapid changes and great fluctuations of total ozone can be detected at the observation site location and are sensitive to the dynamic and chemical changes of PSCs.

As a spectroscopic technique, differential optical absorption spectroscopy (DOAS) has been proven to be powerful and has been widely used to monitor a variety of atmospheric trace gases (Stutz and Platt, 1997; Meller and Moortgat, 2000; Platt and Stutz, 2008). Zenith Scattered Light-DOAS (ZSL-DOAS) is suitable for measuring stratospheric gases, such as stratospheric $NO_2$ and $O_3$ (Pommereau, 1982; Perner et al., 1994). Since the 1970s, numerous spaceborne UV detection instruments (such as Ozone Monitoring Instrument (OMI), Global Ozone Monitoring Experiment 2 (GOME-2), and Microwave Limb Sounder (MLS)) have been launched to observe global trace gases, and their observations have provided comprehensive information on ozone holes and changes (Sonkaew et al., 2013; Zhang et al., 2015; Kuttippurath and Nair, 2017). Some advantages of ZSL-DOAS are that it has low energy consumption and can be unattended, and it is less affected than satellite-based instruments by changes of meteorological conditions in the boundary layer, temperature, and clouds.

In this study, daily variations of ozone vertical column densities (VCDs) are retrieved by ZSL-DOAS, and a correlation analysis is performed between the ZSL-DOAS measurements and OMI, GOME-2 observations and Modern-Era Retrospective analysis for Research and Applications version 2 (MERRA-2). Combining observed ozone VCDs and low-stratospheric PV profiles, the cause of ozone depletion leading to ozone holes from September to October in 2017 and 2018 in the experiment region (62.22°S, 58.96°W) at the edge of the polar vortex is investigated. The aim of this study is to analyze the correlation between ozone depletion and PV at the edge of the polar vortex, where ozone depletion is more sensitive to changes in PV.

## 2. Experiment design and data analysis

### 2.1. *Experiment site*

The experiment site and DOAS instrument are shown in Fig. 1. The red star is the location of Chinese Great Wall Station (62.22°S, 58.96°W) in Fildes Peninsula, South Shetland Islands. The red region is the area of the OMI pixel, and the yellow region is the area of the GOME-2 pixel.

The ground-based passive DOAS system used in this experiment is composed of key parts such as a prism, telescope, motor, filter, CCD spectrometer, and computer. The wavelength range of the spectrometer is 290–420 nm, and the spectral resolution is 0.3 nm. In this experiment, the data from zenith direction is used to retrieve the slant column densities (SCDs) of ozone.

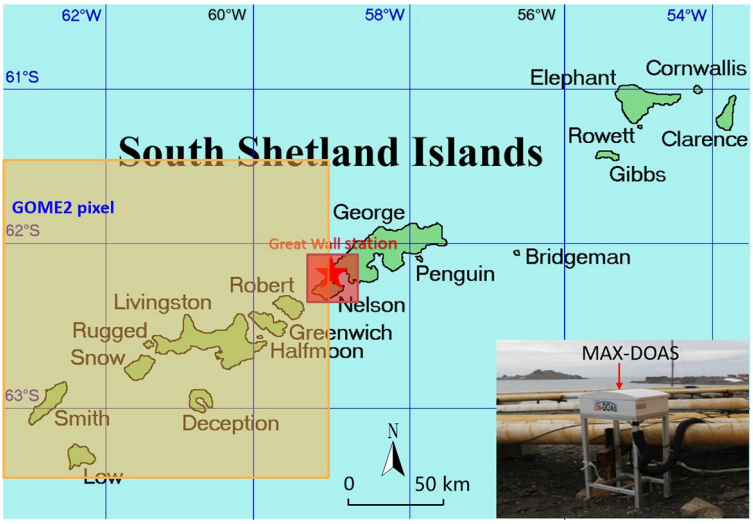


**Fig. 1**. Instrument and experiment site (red star) and pixels of OMI and GOME-2 observations (red and yellow boxes).

### 2.2. *Principles of the DOAS method*

The DOAS method retrieves concentrations of trace gases based on their characteristic absorption and the measured intensity, which is based on Lambert-Beer's law. From Lambert-Beer's law and derivation:

$$\ln\frac{I^*(\lambda)}{I_0(\lambda)} = \sum\left[\sigma_j^*(\lambda)c_jL\right] = \sum\left[\sigma_j^*(\lambda)\mathrm{SCD}_j\right], \quad (1)$$

here, $I_0(\lambda)$ denotes the original luminous intensity of the radiator, $I^*(\lambda)$ represents the measured intensity after filtering through a gas layer of length $L$, $\sigma_j^*(\lambda)$ denotes the broadband absorption cross section at the wavelength $\lambda$, $c_j$ represents the average concentration of gas $j$, $\mathrm{SCD}_j = \int c_jL$ is the slant column density of $j$, and $D = \ln[I^*(\lambda)/I_0(\lambda)]$ is the named differential optical density. The SCD of the desired trace gas can be retrieved through least-squares fitting by Eq. (1).

### 2.3. *Spectral retrieval*

The ozone SCDs are retrieved from the QDOAS software developed by the Royal Belgian Institute for Space Aeronomy (BIRA-IASB) (http://uv-vis.aeronomie.be/software/QDOAS/), with a retrieval wavelength range of 320–340 nm. $O_3$, $NO_2$, $O_4$, and ring (the rotational Raman scattering effect, calculated by Ring.exe of QDOAS) cross sections are considered in the retrieval algorithm, and detailed parameters are shown in Table 1. The daily noon zenith spectrum is used as the reference spectrum for SCD retrieval. Taking the fits of the spectrum from 24 February 2018 as an example (Fig. 2), the differential slant column density (dSCD) of ozone is $5.20\times10^{18}$ molec cm$^{-2}$, with the root mean square (RMS) of spectral fitting residual of $9.76\times10^{-4}$.

### 2.4. *Calculation of ozone VCDs*

The ZSL-DOAS method is powerful in measuring stratospheric gases such as ozone. To convert SCD (related to the viewing angles) into vertical column density (VCD), the Air Mass Factor (AMF) must be introduced. The relationship between SCD and VCD is as follows:

$$\mathrm{AMF} = \frac{\mathrm{SCD}}{\mathrm{VCD}}. \quad (2)$$

AMFs are retrieved from the atmospheric radiative trans-

**Table 1**. Fitting parameters of spectral retrieval.

| Parameter | References |
|---|---|
| $O_3$ | 223 K, 243 K (Bogumil et al., 2003) |
| $NO_2$ | 298 K (VanDaele et al., 1996) |
| $O_4$ | 293 K (Hermans et al., 2003) |
| Ring | Ring.exe |
| Fitting Interval | 320–340 nm |
| Polynomial | 5 |

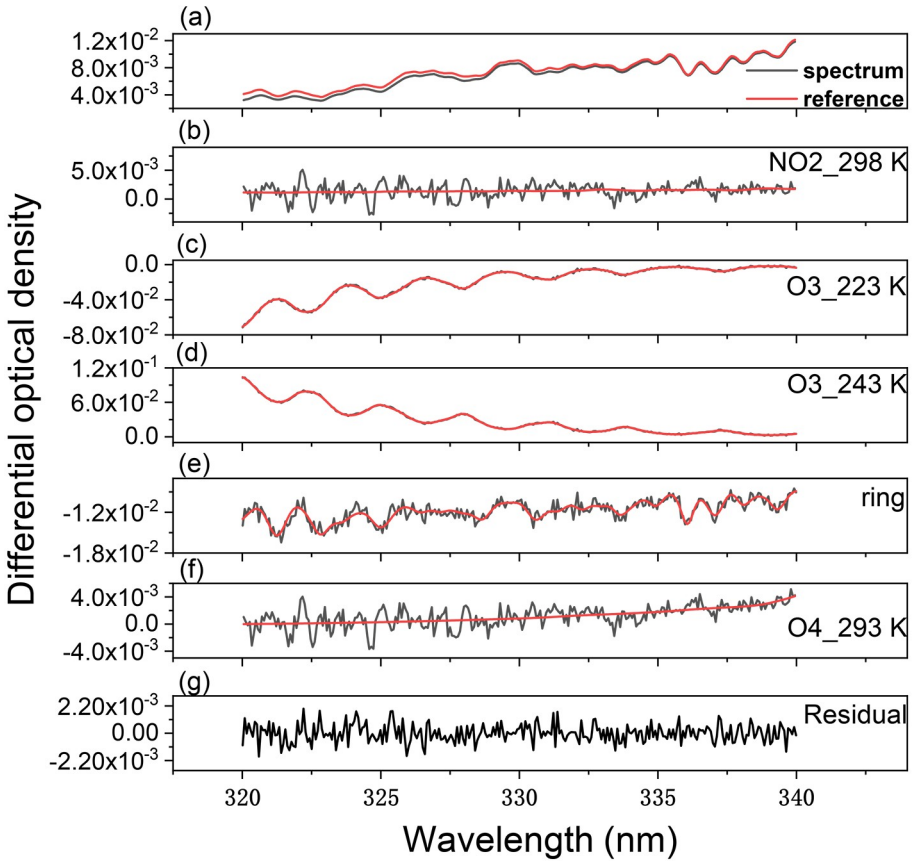


**Fig. 2**. Spectrum fits of ozone on 24 February 2018.

fer model SCIATRAN. The a-priori profiles of ozone, temperature, and pressure used to obtain AMFs are the monthly average profiles from the SCIATRAN profiles database, which are selected by month and latitude. The Fraunhofer absorption, which will have a strong influence on the retrieval of gas concentration, should be removed (Platt and Stutz, 2008). The slant column concentration after deducting Fraunhofer absorption is expressed by the dSCD:

$$\begin{aligned} \mathrm{dSCD}(\alpha,\beta) &= \mathrm{SCD}(\alpha,\beta) - \mathrm{SCD}_{\mathrm{FRS}} \\ &= \mathrm{AMF}(\alpha,\beta)\,\mathrm{VCD} - \mathrm{SCD}_{\mathrm{FRS}}\,. \end{aligned} \quad (3)$$

Here, $\mathrm{SCD}_{\mathrm{FRS}}$ refers to the Fraunhofer absorption part. The above formula is in $y=ax+b$ format, so we can use AMF as the abscissa and dSCD as the ordinate to perform linear fitting, where the slope is VCD and the absolute value of the intercept is the Fraunhofer absorption part. Taking the retrieved data from 24 February 2018 as an example, the linear fit of ozone dSCDs and AMFs on that day is shown in Fig. 3. The calculated ozone VCD is $7.322\times10^{18}$ molec cm$^{-2}$ and the error is $2.232\times10^{16}$ molec cm$^{-2}$. The ozone VCD is calculated by the average of $\mathrm{VCD}_{\mathrm{am}}$ (the VCD of morning) and $\mathrm{VCD}_{\mathrm{pm}}$ (the VCD of afternoon).

The uncertainty of ozone VCD retrieval through the ZSL-DOAS method comes from the retrieval of SCD and AMF. The comprehensive estimation of uncertainty of ozone SCDs is 1.475% (95% confidence interval, $N$ = 76 902). Parameters including SZA (solar zenith angle), surface albedo, a-priori ozone profile, and wavelength, which would influence the values of AMF, are considered. In this study, the SZA used for calculation is between 35° and 80°, and the surface albedo is between 0.08 and 0.6. The a-priori profile of ozone is obtained from the monthly mean climatology. The detailed parameter nodes to estimate the uncertainty of AMF on wavelength are shown in Table 2. The AMF uncertainty caused by wavelength selection is calculated through $(\mathrm{AMF}_\lambda - \mathrm{AMF}_{328})/\mathrm{AMF}_\lambda$, where $\lambda$ denotes wavelength. In the simulated parameter nodes (Table 2), the AMF uncertainty on wavelength is between –4.257% and 4.630%, with the averaged absolute uncertainty being 2.030%. According to the analysis of the OMI ozone product, the variations of AMF influenced by a-priori profiles of ozone are small (2% on the 95% confidence interval) (Bhartia, 2002). Therefore, the averaged AMF uncertainty with this method is calculated through $\sqrt{\mathrm{AMF}^2_{\mathrm{uncertainty\_wave}} + \mathrm{AMF}^2_{\mathrm{profile}}}$, and is 2.85%. The total uncertainty of VCD is 3.21%, based on the error propagation formula as follows:

$$\mathrm{VCD}_{\mathrm{uncertainty}} = \sqrt{\left(\mathrm{SCD}^2_{\mathrm{uncertainty}} + \mathrm{AMF}^2_{\mathrm{uncertainty}}\right)}\,. \quad (4)$$

### 2.5. *Auxiliary data*

The daily ozone VCDs observed by OMI and GOME-2 from January 2017 to February 2020 are obtained for this study. The OMI, launched on 15 July 2004, is onboard the Aura satellite and is a nadir scanning instrument (Xie et al., 2016). The field of view of the OMI can reach 114°, which permits daily global coverage. The OMI can measure ozone in UV (270–380 nm) and VIS (350–500 nm) wavelengths. The spectral resolution of the OMI is 0.5 nm, with high spatial resolution of $13\times24$ km$^2$ (Thomas et al., 2011). The daily ozone VCDs from the OMI (https://disc.gsfc.nasa.gov/) are used to compare with ZSL-DOAS observations.

GOME-2 is a UV/VIS nadir observation spectrometer, which is onboard the MetOp-A satellite and was launched on 19 October 2006 by the European Space Agency (ESA).

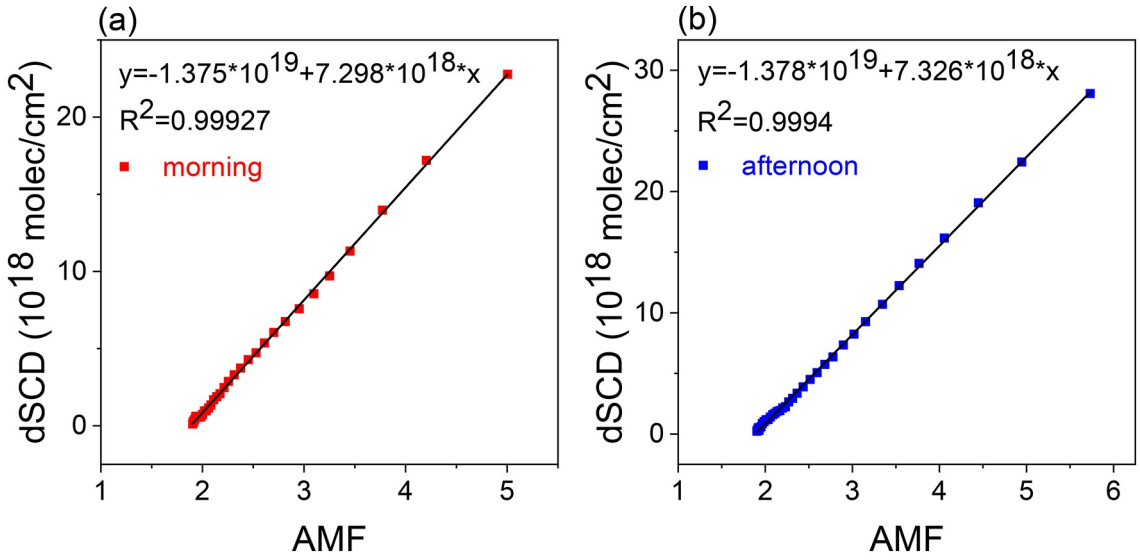


**Fig. 3**. Linear fitting between ozone dSCDs and AMFs for morning (a) and afternoon (b) on 24 February 2018. The correlation coefficients ($R^2$) are 0.99927 and 0.9994. The ozone VCDs for morning and afternoon are $7.298\times10^{18}$ molec cm$^{-2}$ and $7.326\times10^{18}$ molec cm$^{-2}$. The calculated ozone VCD for 24 February 2018 is $7.322\times10^{18}$ molec cm$^{-2}$.

**Table 2**. Parameter nodes to estimate the AMF uncertainty on wavelength.

| Parameters | Nodes |
|---|---|
| SZA | 35°, 40°, 45°, 50°, 55°, 60°, 65°, 70°, 75°, 80° |
| Surface albedo | 0.05, 0.1, 0.2, 0.3, 0.4, 0.5, 0.6 |
| Wavelength | From 320 to 340 nm in 0.5 nm interval |

The ozone data sets of GOME-2 are retrieved by the GOME-type Direct FITting (GODFIT) v4 algorithm. The wavelength range of the GOME-2 instrument is 240–790 nm. The spectral resolution of GOME-2 is 0.2–0.5 nm, with spatial resolution of $80 \times 40$ km$^2$ (Koukouli et al., 2014). The ozone VCDs obtained from the GOME-2 data set (https://avdc.gsfc.nasa.gov/) are daily mean VCDs of the overpass data.

The temperature and ozone profiles used here are obtained from MERRA-2 data and are available every 3 hours. MERRA-2 is an atmospheric reanalysis database, obtained from Goddard Earth Observing System Model, version 5 (GEOS-5) with Atmospheric Data Assimilation System (ADAS) (Ganeshan and Yang, 2019). The spatial resolution of MERRA-2 is $0.5° \times 0.625°$ (lat × lon) with 72 model levels. The ozone profiles and temperature at 50 hPa from MERRA-2 (https://disc.gsfc.nasa.gov/) are daily averages.

The daily PV data used in this study is obtained from ERA Interim datasets from the ECMWF website (https://www.ecmwf.int/). ERA Interim is a 6-hourly reanalysis dataset, which is available from January 1985 to August 2019. The ERA Interim datasets are obtained from the data assimilation system of the Integrated Forecast System (IFS), released in 2006. The spatial resolution of ERA Interim data is $0.25° \times 0.25°$ (lat × lon), with 60 levels in the vertical direction from the surface to 0.1 hPa.

## 3. Results and discussion

### 3.1. *Meteorological conditions*

The meteorological conditions of the Fildes Peninsula are shown in Figs. 4 and 5, which represent temperatures (at 50 hPa) and PV (on isentropic level of 475 K) respectively. $T_{nat}$ denotes the threshold temperature for the formation of PSCs. The temperature trends during the experimental period show that the formation of PSCs began around June, which corresponds to the development of the polar vortex in early winter (Frieβ et al., 2005). Additionally, the overall temperature of 2019 was higher than 2018 and 2017 and had an early termination of low temperatures, which led to the short existence of PSCs.

PV is used to represent the capacity for an air mass to rotate in the atmosphere and to define the edge of the polar vortex. PV is calculated using other parameters such as temperature, wind field, etc. The units of PV (potential vorticity units, PVU) are a combination of SI units (K m$^2$ kg$^{-1}$ s$^{-1}$), where 1 PVU = $10^{-6}$ K m$^2$ kg$^{-1}$ s$^{-1}$. In Fig. 5, the 475 K potential temperature surface, which corresponds to the lower stratosphere, is used as the criterion to define the edge of polar vortex (Paschou et al., 2020), and blue lines denote the PV of the Fildes Peninsula and red lines denote the PV of the vortex edge. Nash's criterion, where the gradient of PV is the highest of the southern hemisphere along the equivalent latitude (Nash et al., 1996), is used to determine the edge of the polar vortex. The blue line being below (above) the red line indicates that the Fildes Pen-

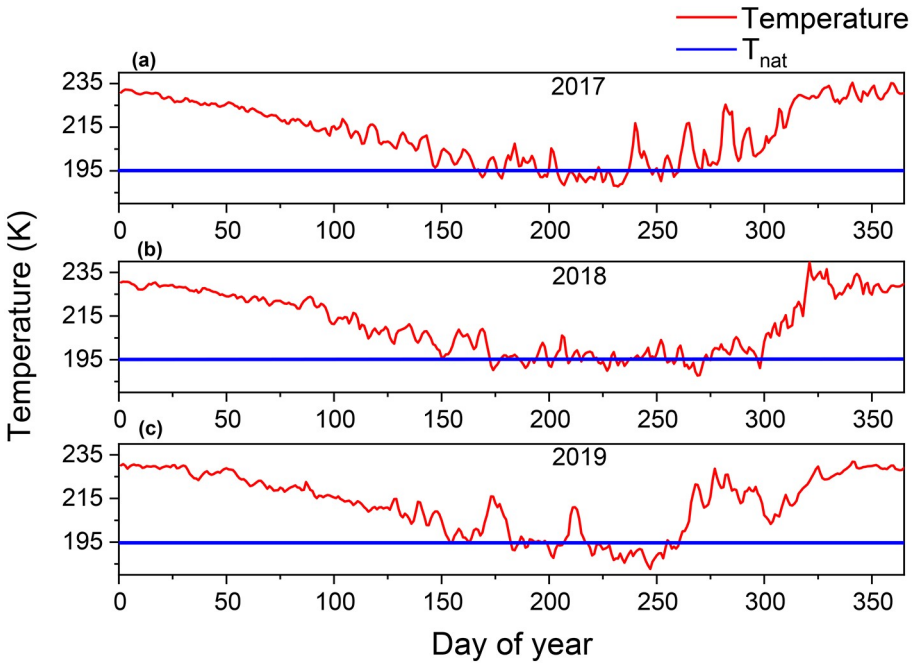


**Fig. 4**. Temperatures (at 50 hPa) over Fildes Peninsula from 2017 to 2019, where the blue lines denote the threshold temperature for the formation of PSCs.

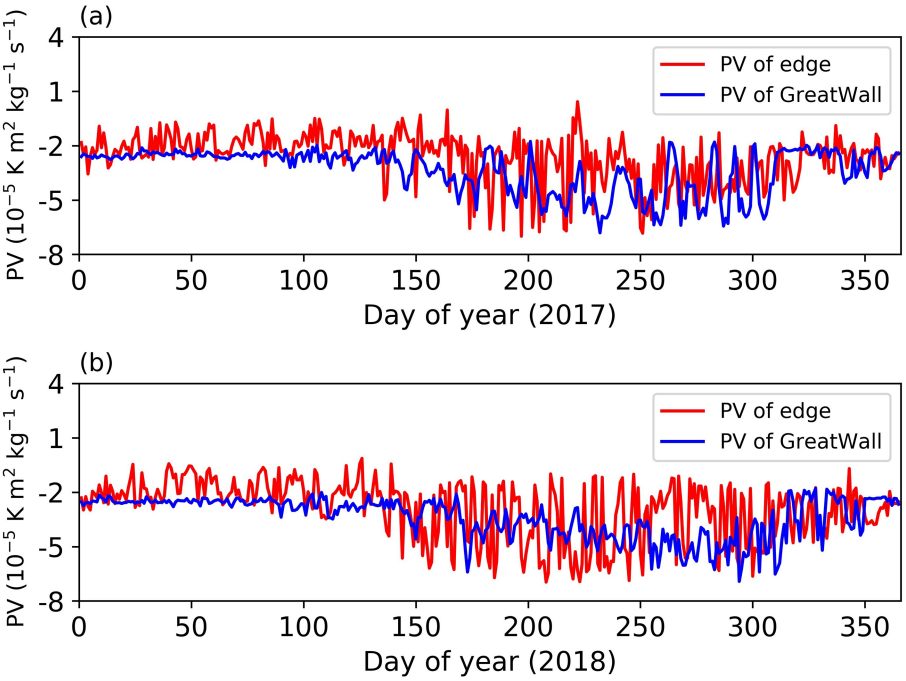


**Fig. 5**. PV (on isentropic level of 475 K) of the Fildes Peninsula and vortex edge, where red and blue lines denote PV of vortex edge (calculated by Nash's criterion) and Fildes Peninsula, respectively. (a) The PV in 2017. (b) The PV in 2018.

**Table 3**. The number of days inside and outside the polar vortex.

| Date | Days inside polar vortex | Days outside polar vortex |
|---|---|---|
| 2017 | 273 | 92 |
| 2018 | 235 | 130 |
| 2017.9–10 | 39 | 22 |
| 2018.9–10 | 45 | 16 |

insula is located inside (outside) of the polar vortex. The number of days inside and outside the polar vortex boundary in 2017 and 2018 are shown in Table 3.

### 3.2. *Results of ozone VCDs*

Satellite ozone observations may have large biases at high latitudes, especially when the SZAs are large. Therefore, the SZAs used to obtain ozone VCDs from satellite observations are less than 86°. The ZSL-DOAS observations in this study can be used to validate the satellite observations at high latitude.

The ozone VCDs retrieved from the ZSL-DOAS instrument, the MERRA-2 dataset and satellite observations from OMI and GOME-2 from January 2017 to February 2020 are shown in Fig. 6a, where the black line located at 220 DU (1 DU = $2.69\times10^{16}$molec cm$^{-2}$) denotes the threshold for an ozone hole (Bodeker et al., 2002). The biases between OMI, GOME-2, MERRA-2, and ZSL-DOAS are shown in Fig. 6b. The standard deviations between GOME-2, MERRA-2, and ZSL-DOAS are shown in Fig. 6c. OMI and GOME-2 are nadir observations that are different from the zenith observation method of ZSL-DOAS. The ozone VCDs of satellite observations could only be obtained at overpass times (1330 LST and 0930 LST), which may have led to the large biases and standard deviations when ozone fluctuated greatly on that day.

The averaged ozone VCDs and ozone hole days for 2017, 2018, and 2019 over the Fildes Peninsula are shown in Table 4. Ozone VCDs start to decline around July with a comparable gradient (around 1.4 DU d$^{-1}$), which is in agreement with the formation of PSCs in Antarctic winter. Ozone VCDs decline further in the spring, with severe ozone depletion in September and October, and then gradually return to normal levels. During the severe ozone depletion periods in September and October, which lead to the ozone holes (<220 DU), there is a correlation between the polar vortex and ozone concentration, which is discussed in detail in section 3.3. The linear fits of the retrieved ozone VCDs with OMI and GOME-2 satellite observations and the MERRA-2 dataset are shown in Fig. 7. The correlation coefficients ($R^2$) are 0.86, 0.94, and 0.90, respectively.

### 3.3. *Influence of PV on ozone depletion*

The sign of PV is negative in Antarctica while positive in the Arctic. The absolute value of PV is generally greater inside the polar vortex. The PSCs formed inside the polar vortex can activate the halogen species, which lead to severe ozone depletion. The PV, temperatures (at 50 hPa), and retrieved ozone VCDs from September to October during the observation period are shown in Fig. 8. As shown in Figs. 8a–d, the trend of PV and ozone VCDs is similar. In other words, PV is positively correlated with the ozone VCDs. The ozone VCDs fluctuate between 170–405 DU from September to October of 2017. The fluctuations in

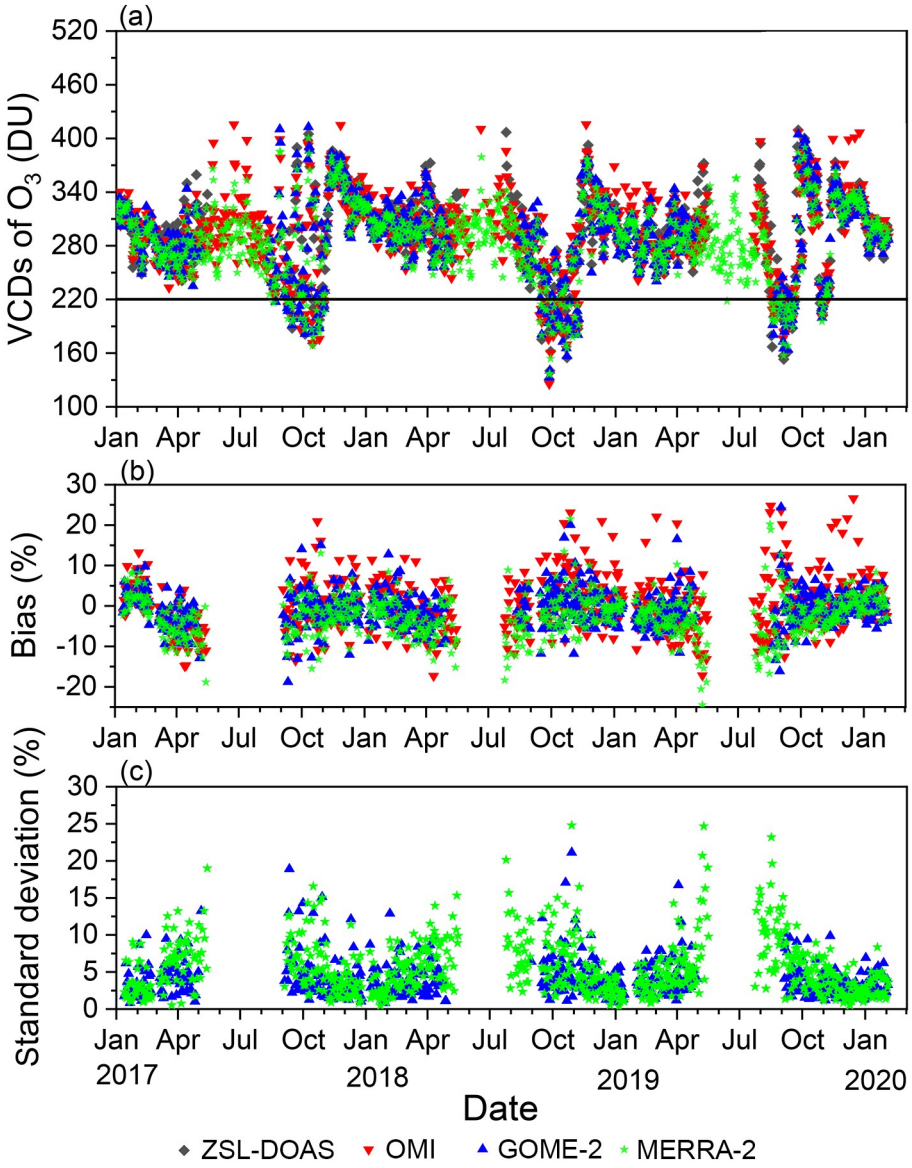


**Fig. 6**. (a) The ozone VCDs from ZSL-DOAS, OMI, GOME-2, and MERRA-2. The black line denotes the threshold for ozone holes. (b) The biases of OMI, GOME-2, and MERRA-2. (c) The standard deviations of GOME-2 and MERRA-2.

**Table 4**. Averaged ozone VCDs and ozone hole days.

| Date | Average ozone VCDs (DU) | Ozone hole days |
|---|---|---|
| 2017 | 295.85 | 16 |
| 2017.9–10 | 260.76 | 15 |
| 2018 | 289.32 | 30 |
| 2018.9–10 | 215.13 | 25 |
| 2019 | 294.04 | 29 |
| 2019.9–10 | 283.38 | 22 |

2018 are between 150–290 DU. The relationship between PV and ozone VCDs is more obvious in 2017 with greater fluctuations. As shown in Fig. 8a, ozone recovers to its peak values on 22 September, 9 October, 19 October, and 28 October 2017, when Fildes Peninsula is fully outside of the polar vortex. The retrieved ozone VCDs fluctuate with the same pattern as the temperatures at 50 hPa, which means ozone is depleted inside the polar vortex, where the temperature is lower. Therefore, the polar vortex has a strong influence on stratospheric ozone depletion during Antarctic spring.

Ozone and PV profiles above the Fildes Peninsula during spring of 2017 and 2018 are analyzed as well. The averaged ozone profiles during the ozone hole periods and non-ozone hole periods from September to October in 2017 are shown in Fig. 9. The averaged ozone profiles and the percentage of ozone loss at different heights indicate that the maximum ozone loss is about 63% at the height of 19.5 km. PV might differ by more than a factor of ten for different heights in the lower stratosphere, which indicates that a small and sensitive height layer should be chosen to discuss its influence on ozone depletion. Therefore, the profile

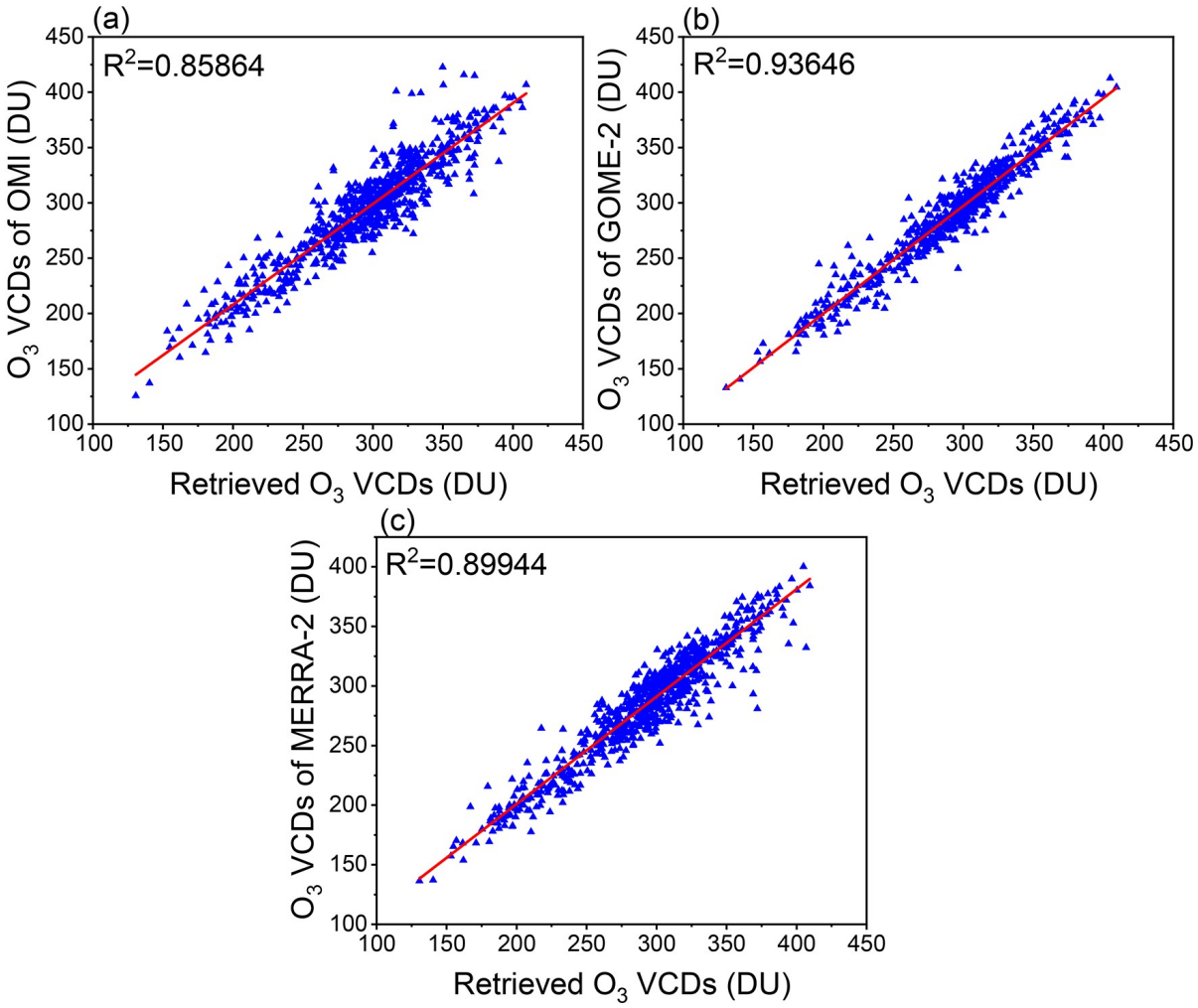


**Fig. 7**. Scatter plots and linear fit of retrieved ozone VCDs with (a) OMI, (b) GOME-2, and (c) MERRA-2.

height of 19–20 km, where the photochemical reactions destroying ozone are most severe, was chosen.

Since the observation site is located near the edge of the polar vortex, it is sensitive to the changes of the polar vortex. The synchronized change between ozone and PV indicates the critical influence of the polar vortex on ozone depletion. The profiles of ozone and PV at the height of 19–20 km from September to October in 2017 and 2018 are shown in Fig. 10. The ozone concentration at the height of 19–20 km fluctuates between 0.65–6.87 ppmv and 0.54–7.30 ppmv in 2017 and 2018, respectively. The absolute value of PV shows an obvious increase when the ozone concentration decreases. The ozone depletion in Antarctic spring, which leads to the formation of ozone holes, is closely related to PV. Located at the edge of the polar vortex, the observed data will provide a basis for further analysis and prediction of the inter-annual variation of stratospheric ozone in future.

## 4. Conclusion

In this study, daily ozone VCDs are retrieved by ZSL-DOAS from ground-based DOAS instrument observations and then linearly fitted with satellite observations from OMI and GOME-2 and reanalysis data from MERRA-2. The correlation coefficients ($R^2$) are 0.86, 0.94, and 0.90 respectively, which validate the satellite observations and MERRA-2 dataset for this area.

Each spring during the observation period, occurrences of ozone holes over the Fildes Peninsula were detected when the daily ozone VCDs fluctuated sharply. Especially in September 2017, the daily fluctuations of ozone VCDs reached up to 100 DU. The ozone VCDs began to decrease in early winter with a comparable gradient (1.4 DU $d^{-1}$) throughout the observation period, corresponding with the formation of PSCs. The ozone concentration began to recover at the end of October, and returned to normal levels after November.

In this study, PV was used as an indicator for analysis because it was positively correlated with ozone concentration over Fildes Peninsula in spring. The polar vortex of Antarctic spring has a strong influence on stratospheric ozone depletion.

It should be noted that the uncertainty estimation of the AMF calculation is preliminary, and the uncertainty caused

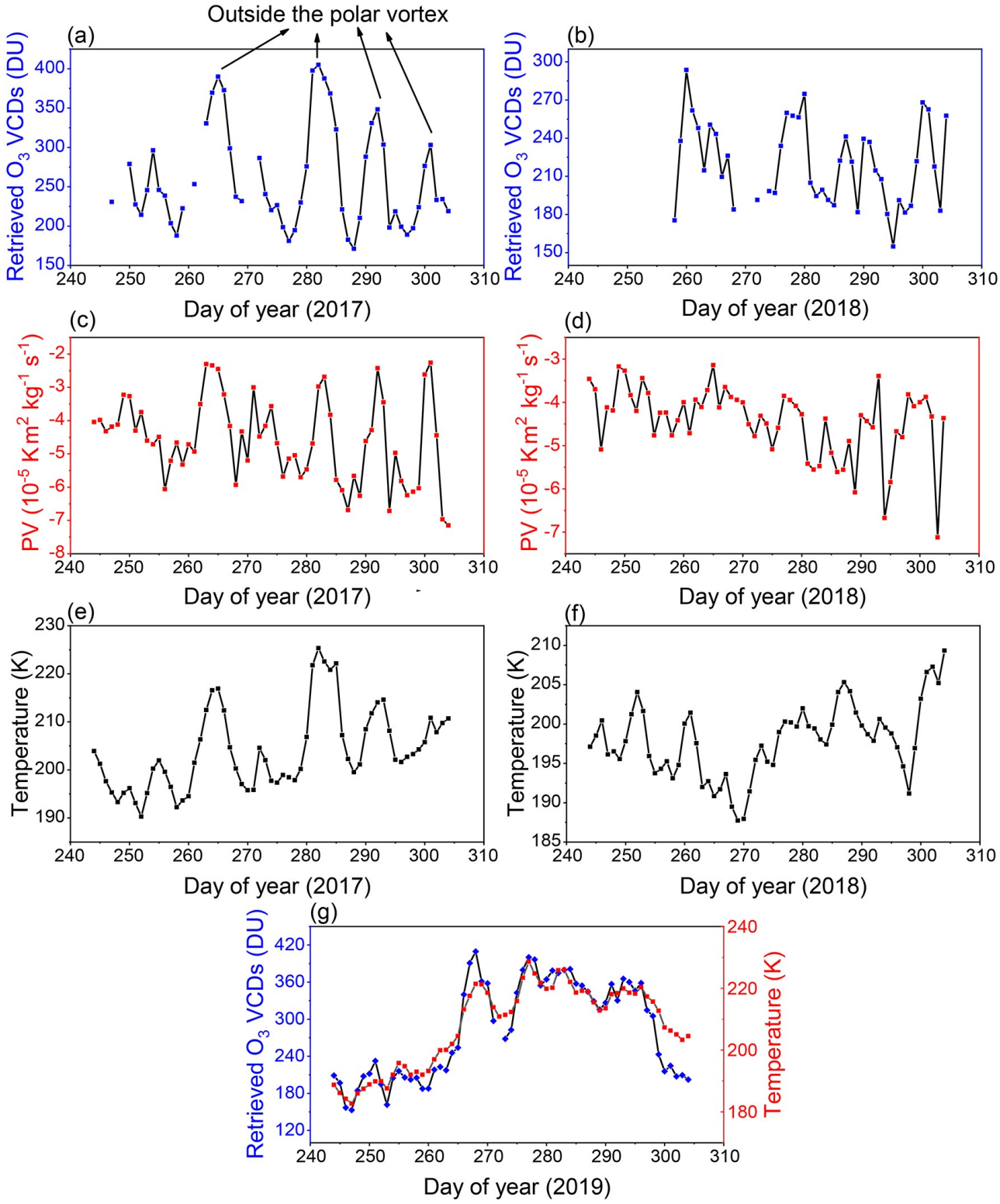


**Fig. 8**. Ozone VCDs, PV, and temperatures (at 50 hPa) from September to October during the observation period: (a) retrieved ozone VCDs from September to October in 2017; (b) retrieved ozone VCDs from September to October in 2018; (c) PV (at 50 hPa) from September to October in 2017; (d) PV (at 50 hPa) from September to October in 2018; (e) temperature (at 50 hPa) from September to October in 2017; (f) temperature (at 50 hPa) from September to October in 2018; and (g) retrieved ozone VCDs and temperature (at 50 hPa) from September to October in 2019.

by the a-priori ozone profiles needs further analysis. More accurate a-priori ozone profiles (like column-dependent total ozone profiles) and a better reference spectrum (from direct-sun data) will be used in future research.

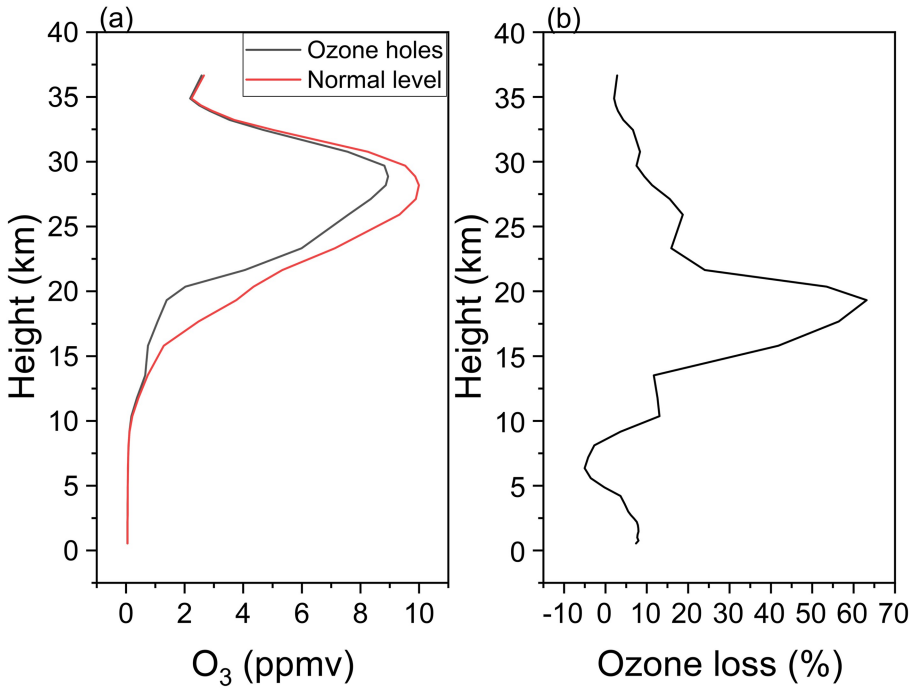


**Fig. 9**. (a) Averaged ozone profiles during the ozone hole periods and non-ozone hole periods from September to October in 2017. (b) The percentage of ozone loss at different heights calculated by (a).

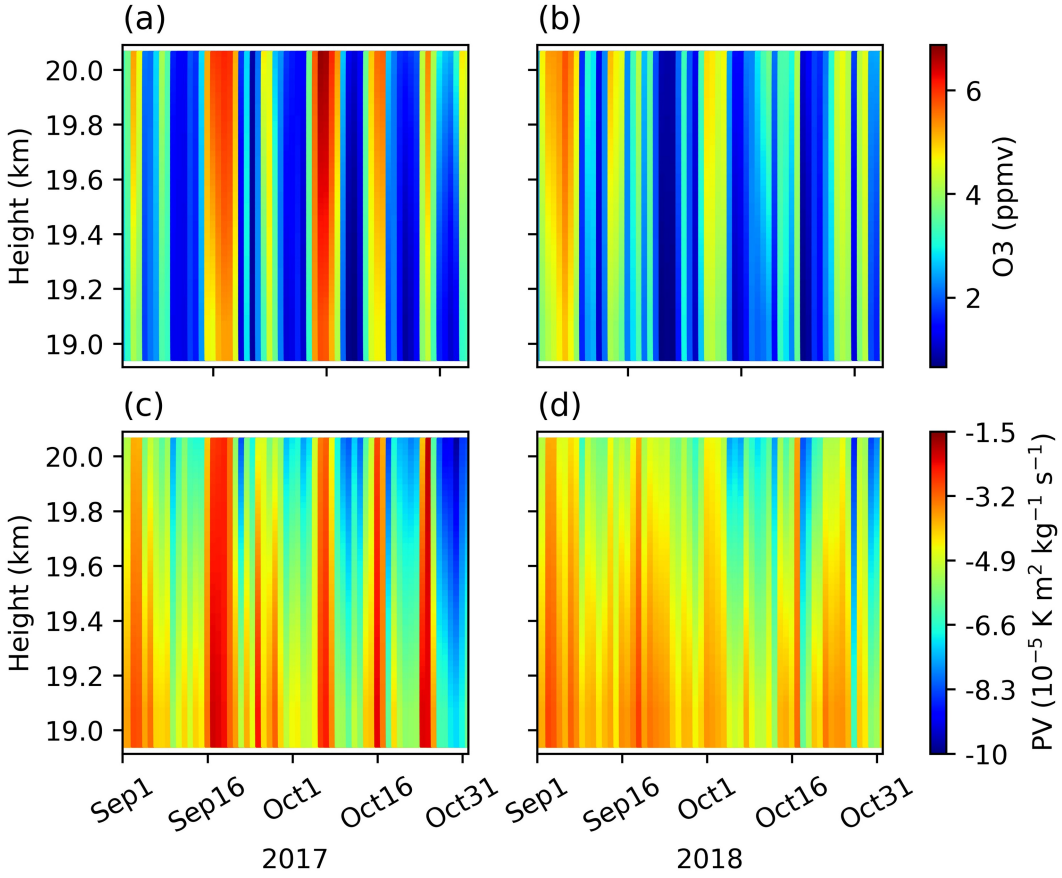


**Fig. 10**. Profiles of ozone and PV from September to October in 2017 and 2018, at the height of 19–20 km: (a) profile of ozone in 2017; (b) profile of ozone in 2018; (c) profile of PV in 2017; and (d) profile of PV in 2018.

Observation of ozone VCDs over Fildes Peninsula will be continually conducted to observe the long-term ozone trends in this region. The observations conducted in this study are also valuable for validating modelled ozone concentrations in this region and contribute to better understanding of ozone recovery and stratosphere-troposphere exchange over the polar vortex edge area.

***Acknowledgements***. This research was financially supported by the National Natural Science Foundation of China (Grant Nos. 41676184 and 41941011). The authors gratefully acknowledge ECMWF (https://www.ecmwf.int/) for providing ERA-Interim reanalysis data and GES-DISC (https://disc.gsfc.nasa.gov/) for providing MERRA-2 data. The authors thank the staff of Great Wall Station for their kind help. The authors acknowledge three anonymous referees for their help on the improvement of the manuscript.

## REFERENCES

Bhartia, P. K., 2002: "OMI Algorithm Theoretical Basis Document: Volume Ⅱ, OMI Ozone Products", ATBD-OMI-02, August. [Available online from https://docserver.gesdisc.eosdis.nasa.gov/repository/Mission/OMI/3.3_ScienceDataProductDocumentation/3.3.4_ProductGenerationAlgorithm/ATBD-OMI-02.pdf]

Bodeker, G. E., H. Struthers, and B. J. Connor, 2002: Dynamical containment of Antarctic ozone depletion. *Geophys. Res. Lett.*, **29**(7), 1098, https://doi.org/10.1029/2001GL014206.

Bogumil, K., and Coauthors, 2003: Measurements of molecular absorption spectra with the SCIAMACHY pre-flight model: Instrument characterization and reference data for atmospheric remote-sensing in the 230–2380 nm region. *Journal of Photochemistry and Photobiology A: Chemistry*, **157**(2–3), 167–184, https://doi.org/10.1016/S1010-6030(03)00062-5.

Čížková, K., K. Láska, L. Metelka, and M. Staněk, 2019: Intercomparison of ground- and satellite-based total ozone data products at Marambio base, Antarctic Peninsula region. *Atmosphere*, **10**(11), 721, https://doi.org/10.3390/atmos10110721.

Drdla, K., and R. Müller, 2012: Temperature thresholds for chlorine activation and ozone loss in the polar stratosphere. *Annales Geophysicae*, **30**(7), 1055–1073, https://doi.org/10.5194/angeo-30-1055-2012.

Farman, J. C., B. G. Gardiner, and J. D. Shanklin, 1985: Large losses of total ozone in Antarctica reveal seasonal $ClO_x/NO_x$ interaction. *Nature*, **315**, 207–210, https://doi.org/10.1038/315207a0.

Frieβ, U., K. Kreher, P. V. Johnston, and U. Platt, 2005: Ground-based DOAS measurements of stratospheric trace gases at two Antarctic stations during the 2002 ozone hole period. *J. Atmos. Sci.*, **62**(3), 765–777, https://doi.org/10.1175/JAS-3319.1.

Ganeshan, M., and Y. K. Yang, 2019: Evaluation of the Antarctic boundary layer thermodynamic structure in MERRA2 using dropsonde observations from the concordiasi campaign. *Earth and Space Science*, **6**, 2397–2409, https://doi.org/10.1029/2019EA000890.

Hegglin, M. I., and T. G. Shepherd, 2009: Large climate-induced changes in ultraviolet index and stratosphere-to-troposphere ozone flux. *Nature Geoscience*, **2**, 687–691, https://doi.org/10.1038/ngeo604.

Hermans, C., A. C. Vandaele, S. Fally, M. Carleer, R. Colin, B. Coquart, A. Jenouvrier, and M. F. Merienne, 2003: Absorption cross-section of the collision-induced bands of oxygen from the UV to the NIR. *Weakly Interacting Molecular Pairs: Unconventional Absorbers of Radiation in the Atmosphere*, C. Camy-Peyret and A. A. Vigasin, Eds., Springer, 193–202, https://doi.org/10.1007/978-94-010-0025-3_16.

Kokhanovsky, A. A., M. Lamare, and V. Rozanov, 2020: Retrieval of the total ozone over Antarctica using Sentinel-3 ocean and land colour instrument. *Journal of Quantitative Spectroscopy and Radiative Transfer*, **251**, 107045, https://doi.org/10.1016/j.jqsrt.2020.107045.

Koukouli, M. E., and Coauthors, 2014: Intercomparison of Metop-A $SO_2$ measure- ments during the 2010–2011 Icelandic eruptions. *Annals of Geophysics*, **57**, 2110, https://doi.org/10.4401/ag-6613.

Kuttippurath, J., and P. J. Nair, 2017: The signs of Antarctic ozone hole recovery. *Scientific Reports*, **7**, 585, https://doi.org/10.1038/s41598-017-00722-7.

Li, G., Y. K. Tan, C. Y. Li, S. C. Chen, T. Bai, D. Y. Yang, and Y. Zhang, 2015: Characteristics of boreal winter total ozone distribution in the northern hemisphere and their relationship with stratospheric temperature during recent 30 years. *Chinese Journal of Geophysics*, **58**(5), 213–228, https://doi.org/10.1002/cjg2.220168.

Lu, X., and Coauthors, 2019: Surface and tropospheric ozone trends in the Southern Hemisphere since 1990: Possible linkages to poleward expansion of the Hadley circulation. *Science Bulletin*, **64**, 400–409, https://doi.org/10.1016/j.scib.2018.12.021.

Marsing, A., and Coauthors, 2019: Chlorine partitioning in the lowermost Arctic vortex during the cold winter 2015/2016. *Atmospheric Chemistry and Physics*, **19**(16), 10 757–10 772, https://doi.org/10.5194/acp-19-10757-2019.

Meller, R., and G. K. Moortgat, 2000: Temperature dependence of the absorption cross sections of formaldehyde between 223 and 323 K in the wavelength range 225-375 nm. *J. Geophys. Res.*, **105**(D6), 7089–7101, https://doi.org/10.1029/1999JD901074.

Nakajima, H., and Coauthors, 2020: Chlorine partitioning near the polar vortex edge observed with ground-based FTIR and satellites at Syowa Station, Antarctica, in 2007 and 2011. *Atmospheric Chemistry and Physics*, **20**(2), 1043–1074, https://doi.org/10.5194/acp-20-1043-2020.

Nash, E. R., P. A. Newman, J. E. Rosenfield, and M. R. Schoeberl, 1996: An objective determination of the polar vortex using Ertel's potential vorticity. *J. Geophys. Res.*, **101**(D5), 9471–9478, https://doi.org/10.1029/96JD00066.

Paschou, P., M. E. Koukouli, D. Balis, C. Lerot, and M. van Roozendael, 2020: The effect of considering polar vortex dynamics in the validation of satellite total ozone observations. *Atmospheric Research*, **238**, 104870, https://doi.org/10.1016/j.atmosres.2020.104870.

Perner, D., A. Roth, and T. Klüpfel, 1994: Groundbased measurements of stratospheric oclo, $NO_2$, and $O_3$ at søndre strømfjord in winter 1991/92. *Geophys. Res. Lett.*, **21**(13), 1367–1370, https://doi.org/10.1029/93GL01871.

Platt, U., and J. Stutz, 2008: *Differential Optical Absorption Spectroscopy: Principles and Applications*. Springer, 568 pp, https://doi.org/10.1007/978-3-540-75776-4.

Pommereau, J. P., 1982: Observation of $NO_2$ diurnal variation in the stratosphere. *Geophys. Res. Lett.*, **9**(8), 850–853, https://doi.org/10.1029/gl009i008p00850.

Solomon, S., D. J. Ivy, D. Kinnison, M. J. Mills, R. R. Neely III, and A. Schmidt, 2016: Emergence of healing in the Antarctic ozone layer. *Science*, **353**(6296), 269–274, https://doi.org/10.1126/science.aae0061.

Sonkaew, T., S. von Savigny, K. U. Eichmann, M. Weber, A. Rozanov, H. Bovensmann, and J. P. Burrows, 2013: Chemical ozone losses in Arctic and Antarctic polar winter/spring season derived from SCIAMACHY limb measurements 2002–2009. *Atmospheric Chemistry and Physics*, **13**(4), 1809–1835, https://doi.org/10.5194/acp-13-1809-2013.

Stutz, J., and U. Platt, 1997: Improving long-path differential optical absorption spectroscopy with a quartz-fiber mode mixer. *Appl. Opt.*, **36**(6), 1105–1115, https://doi.org/10.1364/AO.36.001105.

Thomas, H. E., I. M. Watson, S. A. Carn, A. J. Prata, and V. J. Realmuto, 2011: A comparison of AIRS, MODIS and OMI Sulphur dioxide retrievals in volcanic clouds. *Geomatics, Natural Hazards and Risk*, **2**, 217–232, https://doi.org/10.1080/19475705.2011.564212.

Vandaele, A. C., C. Hermans, P. C. Simon, M. van Roozendael, J. M. Guilmot, M. Carleer, and R. Colin, 1996: Fourier transform measurement of $NO_2$ absorption cross-section in the visible range at room temperature. *Journal of Atmospheric Chemistry*, **25**(3), 289–305, https://doi.org/10.1007/BF00053797.

Xie, B., H. Zhang, Z. L. Wang, S. Y. Zhao, and Q. Fu, 2016: A modeling study of effective radiative forcing and climate response due to tropospheric ozone. *Adv. Atmos. Sci.*, **33**, 819–828, https://doi.org/10.1007/s00376-016-5193-0.

Zhang, Y. L., Y. Liu, C. X. Liu, and V. F. Sofieva, 2015: Satellite measurements of the Madden-Julian oscillation in wintertime stratospheric ozone over the Tibetan plateau and East Asia. *Adv. Atmos. Sci.*, **32**(11), 1481–1492, https://doi.org/10.1007/s00376-015-5005-y.